Small
www.small-journal.com

In Vitro Primary-Indirect Genotoxicity in Bronchial Epithelial Cells Promoted by Industrially Relevant Few-Layer Graphene

*Michael J. Burgum, Martin J. D. Clift, Stephen J. Evans, Nicole Hondow, Mark Miller, Sandra Bustamante Lopez, Adam Williams, Afshin Tarat, Gareth J. Jenkins, and Shareen H. Doak**

Few-layer graphene (FLG) has garnered much interest owing to applications in hydrogen storage and reinforced nanocomposites. Consequently, these engineered nanomaterials (ENMs) are in high demand, increasing occupational exposure. This investigation seeks to assess the inhalation hazard of industrially relevant FLG engineered with: (i) no surface functional groups (neutral), (ii) amine, and (iii) carboxyl group functionalization. A monoculture of human lung epithelial (16HBE14o$^-$) cells is exposed to each material for 24-h, followed by cytotoxicity and genotoxicity evaluation using relative population doubling (RPD) and the cytokinesis-blocked micronucleus (CBMN) assay, respectively. Neutral-FLG induces the greatest (two-fold) significant increase ($p < 0.05$) in micronuclei, whereas carboxyl-FLG does not induce significant ($p < 0.05$) genotoxicity. These findings correlate to significant ($p < 0.05$) concentration-dependent increases in interleukin (IL)-8, depletion of intracellular glutathione (rGSH) and a depletion in mitochondrial ATP production. Uptake of FLG is evaluated by transmission electron microscopy, whereby FLG particles are observed within membrane-bound vesicles in the form of large agglomerates (>1 µm diameter). The findings of the present study have demonstrated the capability of neutral-FLG and amine-FLG to induce genotoxicity in 16HBE14o$^-$ cells through primary indirect mechanisms, suggesting a possible role for carboxyl groups in scavenging radicals produced via oxidative stress.

1. Introduction

Nanotechnology is the leading science of the 21st century.[1] Engineered nanomaterials (ENMs) are defined by the European Commission (EC) as "a natural, incidental or manufactured material containing particles, in an unbound state or as an aggregate or as an agglomerate and where, for 50% or more of the particles in the number size distribution, one or more external dimensions is in the size range 1 nm - 100 nm."[2] Materials manufactured at the nanoscale ENMs differ from their bulk counterparts in a host of scientifically and industrially relevant ways, largely due to their increased surface area to volume ratio.[3,4] Naturally, this demands interest specifically where human health and environmental exposure are concerned given that ENMs possess unique properties which potentially make them toxic.[5]

Graphene holds significant promise in nanotechnology as it is stronger than diamond and consists of a 2-dimensional (2D) honeycomb lattice of carbon atoms.[6] The unique structure and subsequent properties of graphene hold tremendous potential in material sciences.[7] Of particular and often tested interest are graphene's electrical, thermal, and physical properties, which under experimental conditions have exceeded hypothesized parameters.[8–10] Exploiting the unique physicochemical features offered by graphene derivatives has therefore become of significant interest, specifically its high surface area, which is 2636 $m^2\ g^{-1}$ for monolayer graphene.[11] The large surface area is ideal to support modification by copious functional groups

Dr. M. J. Burgum, Dr. M. J. D. Clift, Dr. S. J. Evans, Prof. G. J. Jenkins, Prof. S. H. Doak
Institute of Life Science, Swansea University Medical School
Swansea University
Singleton Park, Swansea, Wales SA2 8PP, UK
E-mail: s.h.doak@swansea.ac.uk

The ORCID identification number(s) for the author(s) of this article can be found under https://doi.org/10.1002/smll.202002551.

DOI: 10.1002/smll.202002551

Dr. N. Hondow
School of Chemical and Process Engineering
University of Leeds
Leeds LS2 9JT, UK
Dr. M. Miller
Centre for Cardiovascular Science
The University of Edinburgh, Queens Medical Research Institute
Edinburgh EH16 4TJ, UK
Dr. S. B. Lopez, Dr. A. Williams
Department of Physics
Swansea University
Singleton Park, Swansea, Wales SA2 8PP, UK
Dr. A. Tarat
Perpetuus Carbon Technologies
Unit B1, Olympus Court, Millstream Way, Swansea Vale, Llansamlet, Swansea SA70AQ, UK

which can be tailored for desired purposes. For example, recently Li and colleagues engineered graphene oxide (GO) with folic acid and polyethyleneimine to act as a nanocarrier, intended to deliver two copper complexes into the folate-receptor-positive nasopharyngeal carcinoma cell line.[12]

Few-layer graphene (FLG), which can be manufactured in bulk quantities via top-down di-electric barrier discharge of mined graphite, can contain upwards of three atomic layers of graphene. FLG has become commercially successful for its incorporation into composite materials as a reinforcing agent. Introducing sulfate or nitrate between the layers followed by rapid heating can cause a quick increase in internal pressure, thus it is often incorporated into other nanocomposites to enhance their properties.[13] Despite graphene's commercial success however, there remains conflicting theories as to the toxicological potential and the respective cellular damage-mechanisms involved when biological systems are exposed to these materials. There is some evidence to suggest that graphene-based materials exhibit toxicity through the promotion of oxidative stress involving the mitochondria.[14–16] Jarosz and colleagues hypothesized the instigating mechanism to be lipid peroxidation followed by mitochondrial membrane destabilization and subsequent reactive oxygen species (ROS) production, which contributed to the induction of DNA damage. However, little-to-nothing is known currently on the effects of FLG upon mitochondria function, i.e., its capacity to produce ATP, respiratory reserve capacity, the effect of FLG on proton leak in the cells, all of which could be significant in facilitating FLG genotoxic impact. The potential role of graphene surface chemistry and functionalization in dictating toxic responses is also conflicting in the scientific literature. The presence of oxygen groups on the surface of graphene and FLG will result in a large net negative charge density conferred by carboxyl, ester, hydroxyl, and carbonyl groupings. The amplitude of this charge density will later determine how the graphene nanoparticles interact electrostatically with the lipid membrane.[17] Ultimately, GO will interact strongly with positively charged lipid head groups, but weak interactions will occur with neutral or negatively charged lipids. As demonstrated by Hu et al., negatively charged GO undergoes electrostatic repulsion with lipids of the same net charge.[18] Therefore, the appropriate functionalization of graphene and FLG needs to take into consideration their potential for influencing the (geno)toxicity of the material to support safe-by-design approaches during.

The aim of this investigation was to first, comprehensively characterize neutral-, amine-, and carboxyl-FLG before, second, investigating their genotoxic impact upon a 16HBE14o$^-$ monoculture. This cell line was specifically chosen to form a tight barrier model of the bronchoalveolar region, owing to their ability to express epithelial membrane protein 1 (EMP1) which creates strong tight junctions, and thus provide a robust model to replicate lung barrier architecture. This phenotypic trait while not unique to just this cell line represented a better alternative to the BEAS-2B epithelial cell line which does not form tight intercellular junctions.[19] To elucidate potential mechanisms associated with the genotoxicity associated with each ENM, the role of a key (pro)-inflammatory mediator (IL-8), antioxidant depletion, and mitochondrial function were assessed. Amine- and carboxyl-FLG were hypothesized to be less genotoxic than neutral-FLG owing to their functional groups contributing to radical-scavenging mechanisms. Finally, the relationship of how the genotoxic mechanisms relate to the physicochemical characteristics of each ENM was considered, providing a hazard potency ranking.

2. Results

2.1. Physicochemical Characterization

Each ENM (with an emphasis on the FLG materials) underwent extensive physicochemical characterization using a wide array of techniques, this data has been summarized in **Table 1**, with detailed analyses available in the Supporting Information. The hydrodynamic diameters of FLG particles were observed to be larger when dispersed in 10% supplemented culture media as opposed to double-distilled water where the additional amine and carboxyl groups appeared to act as surfactants lowering the hydrodynamic diameter when compared to neutral-FLG. The additional FBS content in media-suspended samples did however increase the hydrodynamic diameter of all FLG materials by ≈217 nm. The effect of surface charge was observed in AFM measurements on water-suspended FLG samples where the presence of amine and carboxyl groups decreased the average sample thickness by 8.53 and 39.57 nm, respectively. This analysis highlighted limitations with AFM as media-suspended samples could not be analyzed due to salt crystals forming while drying. Functional groups had the effect of lowering the average layer number from 50 (neutral-FLG) to 12 and 4 in amine-FLG and carboxyl-FLG, respectively. When suspended in double-distilled water the presence of amine and carboxyl groups decreased the average diameter of agglomerates by 172 and 676.3 nm, respectively. The average agglomerate diameter for neutral-FLG suspended in 10% culture media was decreased by ≈145.7 nm; this effect however was not observed in amine-FLG and carboxyl-FLG. These two ENMs agglomerate diameter was increased by 430.9 and 539.9 nm indicative of the serum proteins within the FBS and additional ENM surface groups undergoing steric hindrance and/or electrostatic interactions, resulting in larger agglomerates. The effect of amine functionalization in the present study gave rise to an unexpected effect, that being to raise the zeta potential to a greater (negative) value than the carboxyl groups. This could be the result of an undesired oxygen-related functional group which may be contributing to the net negative zeta potential, particularly given the oxygen content of amine-FLG was greater than carboxyl-FLG.

Neutral-FLG and carboxyl-FLG generated significant levels of superoxide radicals when assessed with EPR spectroscopy, with the first significant increase observed at 55 μg mL^{-1} (Figure S11a, Supporting Information). Amine-FLG displayed a lower signal, however this is believed to be attributed to a larger presence of carbon radicals that would be overlooked in the EPR experiment, which focused on investigating oxygen-centered radicals. At 100 μg mL^{-1} however all FLG materials generated significant levels of superoxide radicals. Raman spectroscopy revealed high surface defects in neutral- and

Table 1. The role of surface chemistry on the physicochemical characteristics of neutral-FLG, amine-FLG, carboxyl-FLG, and CB particles. By assuming neutral-FLG as a reference ENM, any feature of the functionalized variants which appears in italic indicates an increase and conversely bold indicates a decrease in that specific physicochemical feature. Replicates for each experimental parameter can be found in the materials and methods, where units are not required please read N/A as not applicable. Statistics were not applied to this data set.

Properties	Technique	Unit	Neutral-FLG	Amine-FLG	Carboxyl-FLG	CB
Average primary diameter $n = 121$	SEM	µm	1.03 ± 0.8	**0.98** ± 0.7	**1.14** ± 1.1	0.129 ± 0.3
Weight composition	EDX	%	C (97.4) O (1.93) S (0.31)	**C (88)** *O (9.66)* N (1.74)	**C (92.16)** *O (7.32)* N (0.52)	C (98.94) O (1.06)
Surface charge (H_2O) $n = 3$	Zetasizer Nano ZS	mV	−31.72 ± 1.95	*−41.96* ± 0.86	*−34.36* ± 3.06	−43.7 ± 5.4
Surface charge (10% FBS MEM) $n = 3$		mV	−9.801 ± 0.66	*−9.971* ± 0.71	**−9.76** ± 0.72	−12.4 ± 0.83
Hydrodynamic diameter H_2O $n = 3$	DLS	nm	290.8 ± 302.6	**170.1** ± 97.92	**169.6** ± 76.88	513.3 ± 421.2
Hydrodynamic diameter 10% FBS MEM $n = 3$		Nm	504.7 ± 364.7	**426.4** ± 310.8	**348.2** ± 183.9	347.7 ± 195.1
Presence of Endotoxin $n = 1$	LAL Gel Clot assay	N/A	Negative	Negative	Negative	Negative
Thickness $n = 100$	AFM	nm	94.73 ± 67.94	**86.20** ± 42.16	**55.16** ± 42.22	N/A
Layer number	AFM	nm	50	**12**	**4**	N/A
Particle size H_2O $n = 200$	Plunge freeze SEM	Nm	153.2 ± 19.2	*163.8* ± 21.7	*158.5* ± 19.6	N/A
Particle size media $n = 200$			101.3 ± 16.8	*124.4* ± 13.9	**99.5** ± 15.3	N/A
Agglomerate size H_2O $n = 100$			729.4 ± 317	**557.4** ± 119.9	**543.1** ± 202.3	N/A
Agglomerate size media $n = 100$			583.7 ± 212	*988.3* ± 285.3	*1083* ± 626.6	N/A

carboxyl-FLG originating from in-plane transverse optical phonons at the Dirac points (*K*) of the Brillouin zone, at 1350 cm^{-1} (Figure S11b, Supporting Information). Amine-FLG displayed a sharper G band at 1583 cm^{-1} which split into a second order phonon process at the base of the peak derived from in-plane transverse and in-plane longitudinal optical phonons. 2D bands were present for each FLG material originating from two transverse optical phonons at the Dirac points.

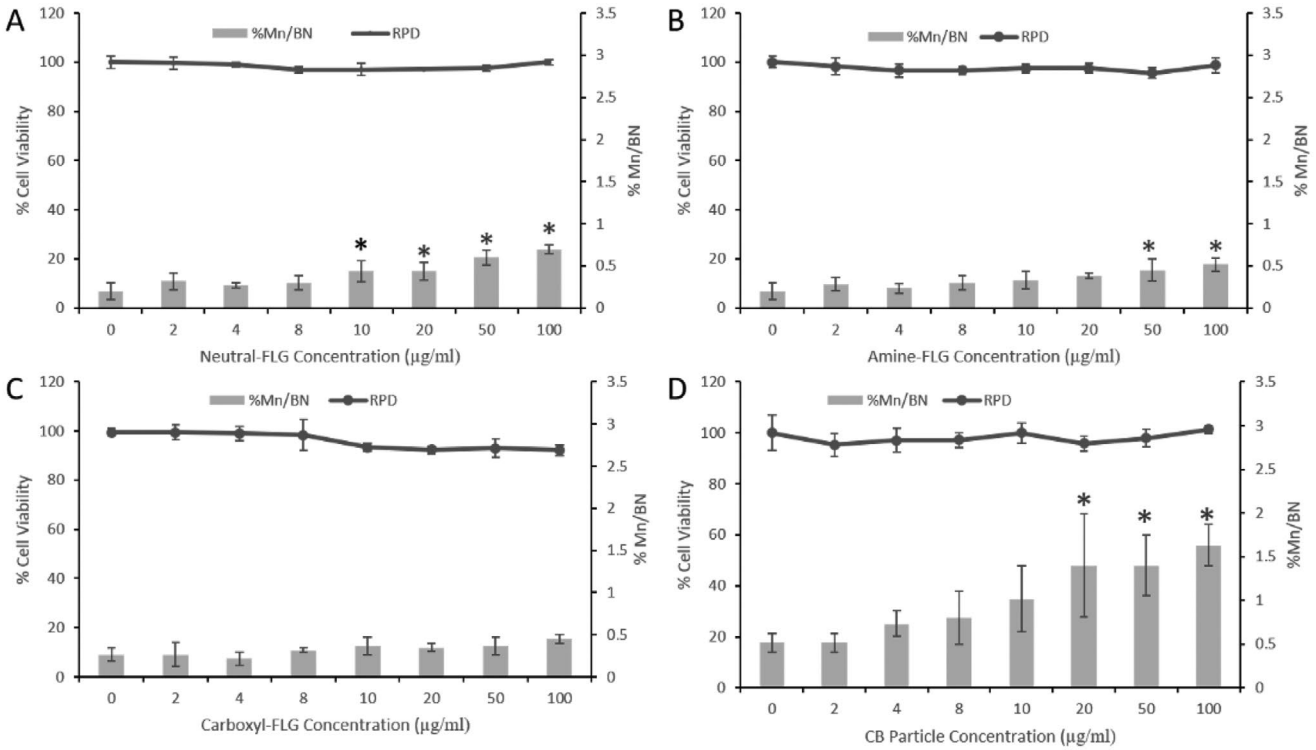

Figure 1. Cytotoxicity and genotoxicity assessment of ENM exposure to 16HBE14o⁻ cells. Cytotoxicity and chromosomal damage were assessed using the RPD and the in vitro CBMN assay respectively following exposure to A) neutral-FLG, B) amine-FLG, C) carboxyl-FLG, and D) CB particles. Results were considered significant (*) when $p < 0.05$. An MMC positive control was included in all experiments and demonstrated a 4.8-fold increase over control (2.51% binucleated cells containing micronuclei (Mn/BN)). All experiments were conducted in triplicate ($N = 3$).

2.2. Assessment of the Cytotoxic and Genotoxic Potential of Each Test ENM

Evaluation of cytotoxicity and genotoxicity induced by neutral-FLG, amine-FLG, carboxyl-FLG, and CB was undertaken by relative population doubling and the in vitro CBMN assay, respectively. No cytotoxicity was observed with any of the tested ENMs, however significant genotoxic responses were recorded following exposures to neutral-FLG, amine-FLG, and CB particles. Genotoxic assessment of neutral-FLG upon 16HBE14o$^-$ demonstrated a potent ability to promote chromosomal damage with all concentrations above the lowest observed genotoxic effect level (LOGEL) of 10 μg mL^{-1} (**Figure 1**A). At the LOGEL concentration there was a twofold increase in DNA damage over control which continued to rise in a concentration-dependent manner reaching 0.43%, 0.6%, and 0.7% micronuclei at 20, 50, and 100 μg mL^{-1}, respectively; at 100 μg mL^{-1} this represented a threefold increase over the negative control. Cells treated with amine-FLG showed two significant responses to ENM exposure at 50 and 100 μg mL^{-1} with respective micronucleus frequencies of 0.45% and 0.51%, indicating greater than twofold increase over control at the highest concentration (Figure 1B). Cells exposed to carboxyl-FLG demonstrated only a small increase in micronuclei witnessed across all tested concentrations, but this did not reach statistical significance (Figure 1C). CB particles promoted a strong genotoxic response with a LOGEL value of 20 μg mL^{-1} and a no observed effect level (NOEL) of 10 μg mL^{-1} (Figure 1D). The three highest concentrations of CB particles demonstrated respective micronucleus frequencies of 1.4%, 1.4%, 1.63%, representing a threefold increase over control at 100 μg mL^{-1}. Thus, the final genotoxicity hazard ranking of the tested materials was CB > neutral-FLG > amine-FLG > carboxyl-FLG.

Chromosomal damage was further evaluated to classify it as either events generated through clastogenicity or aneugenicity with FISH centromeric staining (Figure S14, Supporting Information);, i.e., was the induction of DNA damage the result of chromosome fragmentation (clastogenicity, where the micronucleus contains a chromosome fragment) or loss/gain of whole chromosomes (aneugenicity, the micronucleus contains an entire chromosome). ENMs that elicited significant genotoxicity at 100 μg mL^{-1} showed potential to promote double-stranded DNA breaks and thus chromosome fragments resulting in micronuclei, however, there were also aneugenic responses indicative of entire chromosome loss. Of each tested ENM only amine-FLG promoted significant (*) clastogenicity.

2.3. (Pro)-Inflammatory Response

To investigate the (pro)-inflammatory effect of neutral-FLG, amine-FLG, carboxyl-FLG, and CB, IL-8 ELISAs was performed on supernatants harvested at 16 h (peak IL-8 levels) and 24-h of exposure (end of exposure period). ENM exposures to 16HBE14o$^-$ cells for 16 h promoted a concentration-dependent increase in IL-8 becoming significant at 20 μg mL^{-1} and increasing further at 100 μg mL^{-1} (**Figure 2**A). Control levels of IL-8 (899 pg mL^{-1}) were elevated to 2365 pg mL^{-1} (neutral-FLG), 1767 pg mL^{-1} (amine-FLG), 1994 pg mL^{-1} (carboxyl-FLG), and 1784 pg mL^{-1} (CB) at 100 μg mL^{-1} showing an ≈twofold increase in IL-8 activation at 16 h. At 24 h of exposure the top concentration of ENMs maintained their twofold activation over baseline levels with neutral-FLG, amine-FLG, carboxyl-FLG, and CB promoting IL-8 levels to 2161, 2064, 2134, and 2615 pg mL^{-1}, respectively, although this did not reach significance (Figure 2B). At 100 μg mL^{-1} amine-FLG showed the smallest IL-8 protein expression of all tested ENMs while neutral-FLG at 16 h and CB at 24 h showed the greatest IL-8 protein expression respectively with a potency of neutral-FLG > carboxyl-FLG > CB > amine-FLG at 100 μg mL^{-1}.

2.4. Depletion of Intracellular Glutathione

To determine what oxidative effect neutral-FLG, amine-FLG, carboxyl-FLG, and CB particles may have had, intracellular GSH was quantified via fluorescence following a 24-h exposure period. The initial concentrations of 2 and 4 μg mL^{-1} revealed a slightly beneficial role, promoting GSH levels to an average 6.5 nmol mg^{-1} protein from control (5 nmol mg^{-1} protein) (**Figure 3**A). Concentrations of 8–100 μg mL^{-1} initiated a

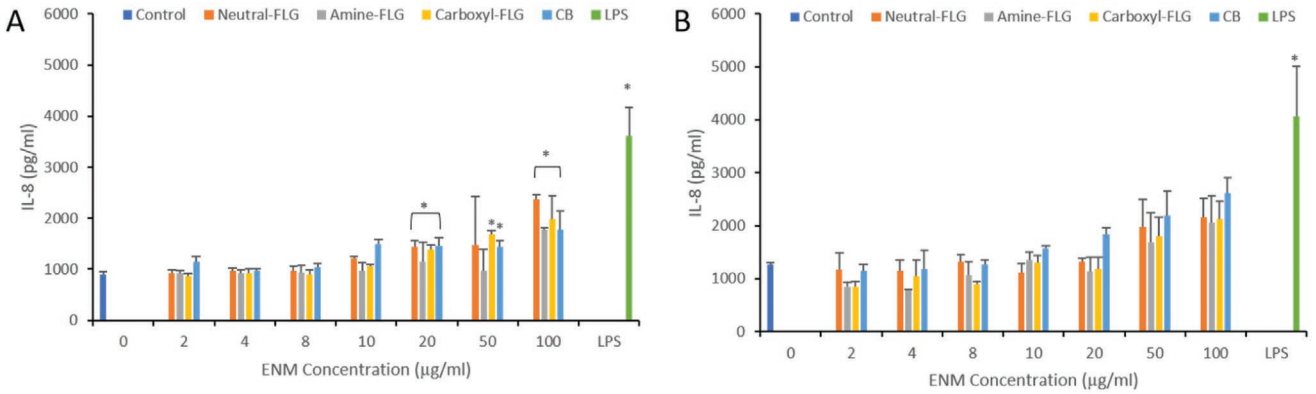

Figure 2. IL-8 (pro)-inflammatory response of 16HBE14o$^-$ cells after exposure to ENMs. IL-8 protein levels after A) 16 h and B) 24 h were elevated in a concentration-dependent trend. IL-8 levels returned to non-significant (*) levels at 24-h of exposure however at 50 μg mL^{-1} and 100 μg mL^{-1} protein levels were still elevated over control levels. LPS at 100 ng mL^{-1} was used as the positive control throughout and the negative control was media only. Results were considered statistically significant (*) when $p < 0.05$ and compared to baseline levels ($N = 3$).

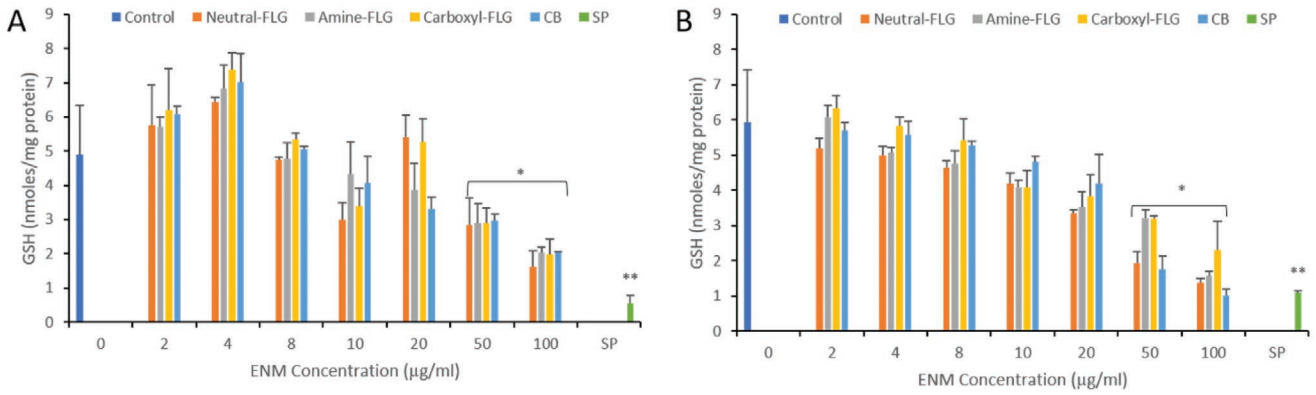

Figure 3. Intracellular reduced glutathione levels measured with monochlorobimane-GSH binding fluorescence after ENM exposures for A) 6 h and B) 24 h. Staurosporine (SP) was used as a positive control at 1 μg mL^{-1} inducing apoptosis in the cells as rapidly as 4 h post-treatment. A concentration-dependent trend was observed with initial significant (*) responses being induced at 50 μg mL^{-1} after 6-h of exposure and being sustained for a further 18-h. Results were considered statistically significant (*) when $p < 0.05$, **$p < 0.01$; $N = 3$.

concentration-dependent decrease in GSH levels which at 50 and 100 μg mL^{-1} represented a two- and fourfold depletion from control levels at 2.8 and 1.6 nmol mg^{-1} protein respectively for each ENM. Following a 24-h exposure period to ENMs the GSH levels in the 16HBE14o^{-} cells showed no sign of recovery after the initial depletion from control levels, with CB reducing GSH by fivefold to 1 nmol mg^{-1} protein at 100 μg mL^{-1} (Figure 3B). Concentrations of 50 and 100 μg mL^{-1} remained significant after 24 h of exposure and a concentration-dependent trend remained evident. Carboxyl-FLG appeared to have the lowest oxidizing capacity with GSH levels rising from 1.98 to 2.3 nmol mg^{-1} protein at 100 μg mL^{-1}. At 24-h of exposure, CB depleted GSH to levels comparable with the positive control Staurosporine, at 1.01 and 1.10 nmol mg^{-1} protein, respectively.

2.5. Oxygen Consumption Rate (OCR), Extracellular Acidification Rate (ECAR), and Mitochondrial Bioenergetics

All ENM concentrations reduced the OCR below control levels except at 4 μg mL^{-1} (**Figure 4**A). This effect was also observed while monitoring the ECAR whereby 4 μg mL^{-1} of each ENM elevated the extracellular acidification rate (Figure 4B). The concentration of 50 μg mL^{-1} proved to be the most potent in depleting the OCR below control cell levels for all test ENM. The ECAR of each ENM and control (0 μg mL^{-1}) shows an elevation over time, however treatment with neutral-FLG (4 μg mL^{-1}) at 27 min showed an initial significant elevation over control rising 1.3-fold from 108 to 147 pmol min^{-1} mg^{-1} protein.

A concentration-dependent trend was observed for all respiratory parameters, becoming significant at 2 μg mL^{-1} (**Figure 5**A–D). Proton leak initially underwent a significant increase at 4 μg mL^{-1} of neutral-FLG before decreasing significantly at 8–50 μg mL^{-1}. Non-mitochondrial respiration showed an increase at low concentrations of 2, 4, 8, and 20 μg mL^{-1} with significant elevation over control levels to respective values of 40, 50, 38.5, and 40 pmol min^{-1} mg^{-1} protein following neutral-FLG and amine-FLG exposures. Basal levels of respiration showed a concentration-dependent significant decrease from 8–50 μg mL^{-1}, however basal levels showed signs of recovery at 100 μg mL^{-1}. Neutral-FLG exposure promoted ATP production at 4 μg mL^{-1}, however this was followed by significant depletions at 8, 10, and 50 μg mL^{-1} with a recovery of ATP production at 100 μg mL^{-1}. The maximal respiration levels of 16HBE14o^{-}

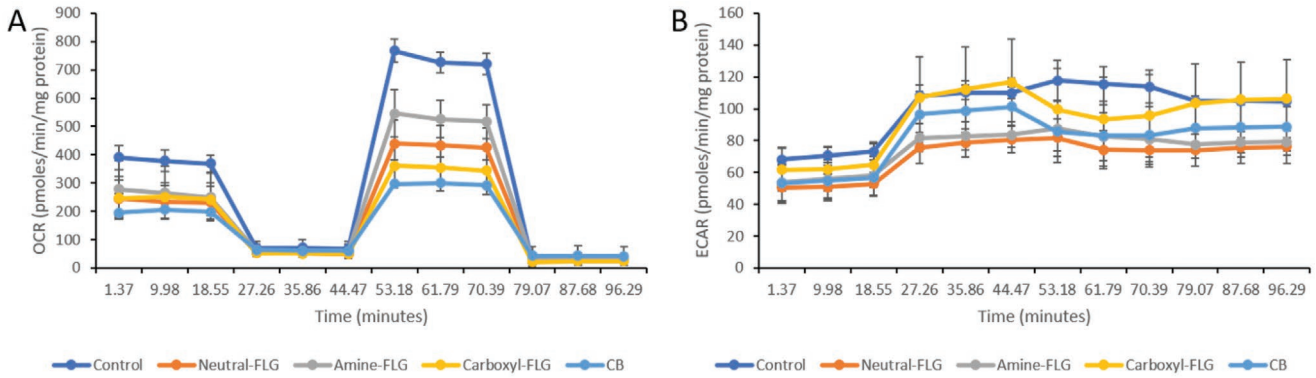

Figure 4. The bioenergetic profile of 16HBE14o^{-} cells exposed to ENMs for 24-h; A) OCR and B) ECAR. Data represents control cells (0 μg mL^{-1}) compared with each test ENM at an exposure concentration of 50 μg mL^{-1}. The effect of ENMs upon 16HBE14o^{-} cells was to lower the oxygen consumption and the extracellular acidification rates respectively. CB particles and carboxyl-FLG, the two most oxidized materials appeared to have the greatest effect overall, $N = 3$.

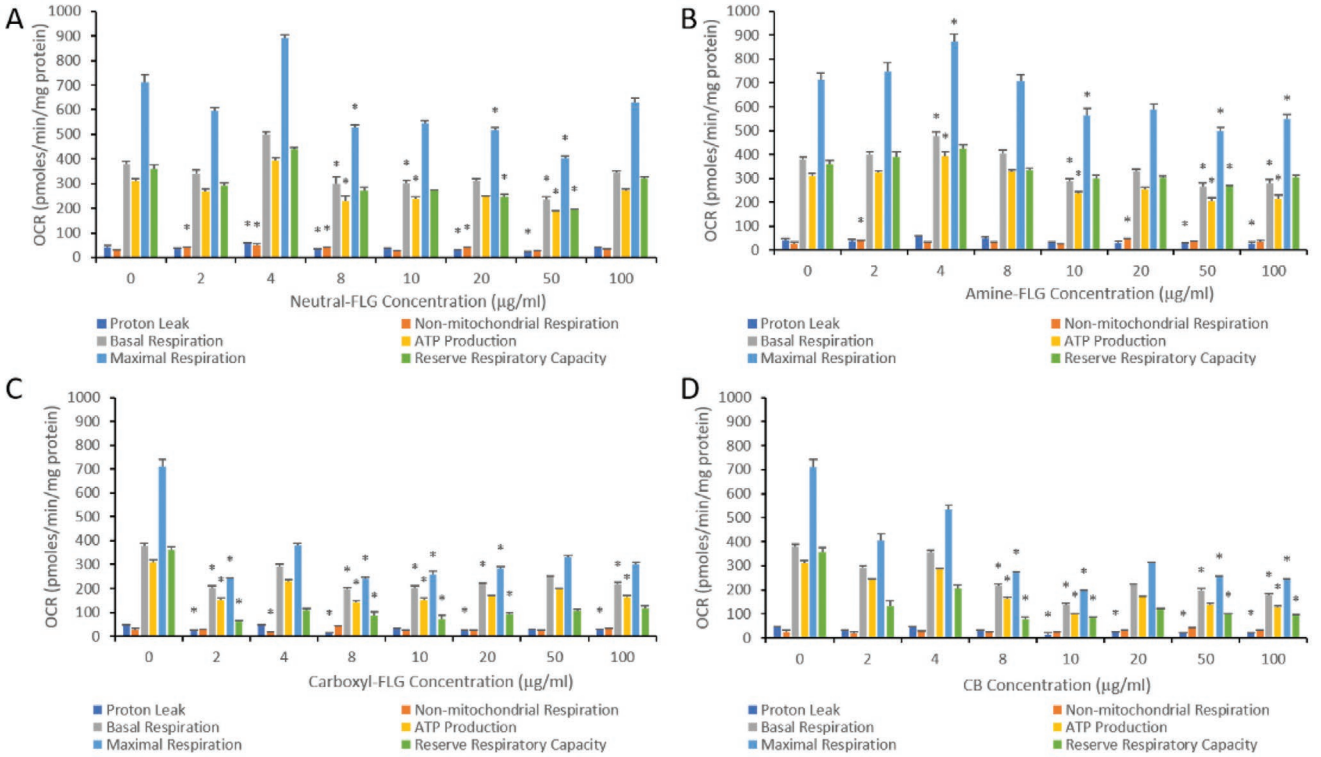

Figure 5. The effect of ENM exposure on 16HBE14o$^-$ bioenergetics where A) neutral-FLG, B) amine-FLG, C) carboxyl-FLG, and D) CB. This data set was derived from initial OCR measurements which utilized chemical compounds Oligomycin (1×10^{-6} M), FCCP (1×10^{-6} M) and a Rotenone/Antimycin A mix (0.5×10^{-6} M). Results were considered statistically significant (*) when $p < 0.05$, $N = 3$.

cells were depleted significantly at 8, 20, and 50 μg mL^{-1}, with respective concentrations of 528, 516, and 404 pmol min^{-1} mg^{-1} protein. Some recovery of maximal respiration was observed at the highest tested ENM concentration.

2.6. Assessment of FLG-Epithelial Cell Interaction

To determine if ENM uptake had taken place during the exposure time, TEM was performed to qualitatively assess how each test material interacted with the 16HBE14o$^-$ cells. This evaluation demonstrated that all test materials were capable of being internalized by 16HBE14o$^-$ cells (**Figure 6**). TEM imaging revealed little uptake of CB particles (not quantified) but particles were also observed in membrane-bound vesicles within cells, not free within the cell cytoplasm. The *z*-axis orientation of some of the FLG materials encapsulated within the cellular vesicles permitted the use of fast Fourier transform (FFT) analysis to measure an interplanar distance of 0.35 nm, thus confirming the internalized ENMs were graphene-based ENMs (Figure S15, Supporting Information). CB particles were presented as largely amorphous carbon at high magnification and thus no FFT analysis was possible.

3. Discussion

This work aimed to explore the genotoxic potential of three FLG materials (neutral-FLG, amine-FLG, and carboxyl-FLG) before exploring the underlying mechanisms of any genotoxic or cytotoxic response observed. By assessing the biological impact of FLG functionalized both without and with amine or carboxyl groups, this study has been to deduce the impact and role of surface chemistry in relation to FLG toxicity to human-derived 16HBE14o$^-$ cells, the key significant responses of which have been summarized in **Table 2**. Cytotoxicity was evaluated in parallel with the genotoxic response, measured with the in vitro CBMN assay after a 24-h exposure period. The data revealed no significant cytotoxicity at any concentration of ENM including 100 μg mL^{-1}. This was consistent with studies on graphene ENMs exposed to murine lung epithelial cell line (FE1) which indicated no cytotoxicity at very high concentrations (200 μg mL^{-1}) as in the study by Bengtson and colleagues.[20,21] A similar finding was observed in the present study with the lack of cytotoxic effects with CB particles. Don Porto Carero and colleagues reported no significant CB cytotoxicity in lung models at low concentrations of 16 μg mL^{-1} in A549 and in THP-1 immune cells.[22] The lack of a cytotoxic response could be attributed to the serum-containing media which have been shown to decrease the cytotoxic effects of nano- and micron-sized materials. One example of the serum effect on A549 cells was performed by Hsiao and Huang using zinc oxide (ZnO) at 50–70 nm and sub-micron particles to treat the alveolar cells in media containing 5 or 10% FBS.[23] The authors noted the highest degree of cytotoxicity in serum-free media in contrast to 5 and 10% FBS-media. The authors suggested that particles in serum-free media would have a higher dose-to-cell ratio resulting from larger particle agglomerates, greater rate of

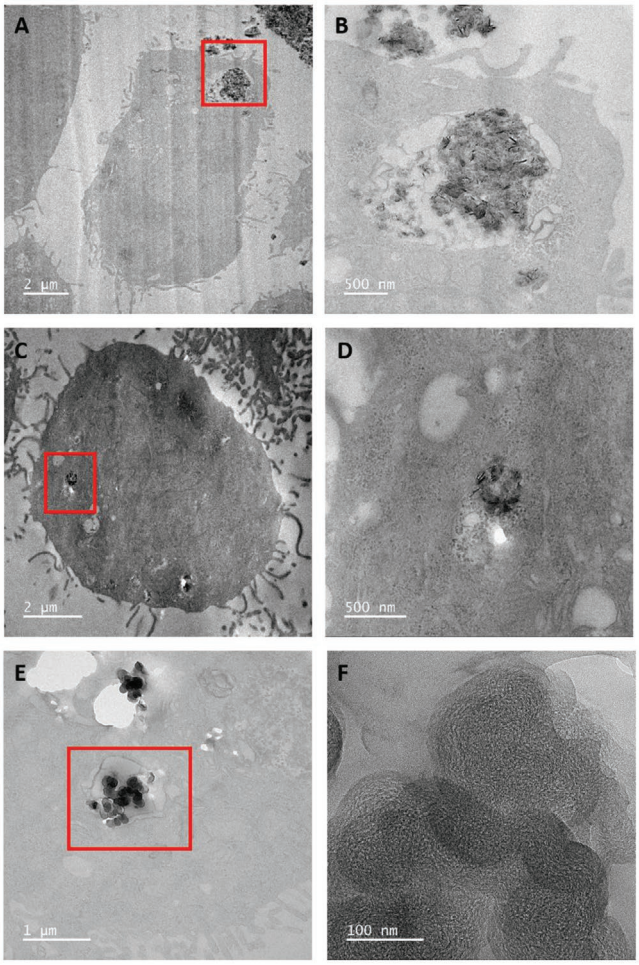

Figure 6. Representative TEM micrographs of 16HBE14o⁻ cells exposed to 20 µg mL^{-1} of ENMs for 24-h. 16HBE14o⁻ cells exposed to A) neutral-FLG, C) carboxyl-FLG, and E) CB (respectively) with higher magnification micrographs of each ((B), (D), and (F), respectively). Uptake was consistent across all particle types whereby ENMs were contained within endocytic vesicles suggesting either phagocytosis or macropinocytosis given the size of the vesicles. Amine-FLG was also observed within membrane-bound vesicles however TEM images were marred during sectioning and have not been presented as a result.

sedimentation, absence of protein corona which can enhance biocompatibility, and lower cell-growth rate.[23,24]

The genotoxicity of carbonaceous ENMs is greatly varied in the literature which could be attributed to numerous factors including cell-line selection, the physicochemical features of the test ENM, the exposure assay, and the exposure time.[25] In the present study, neutral-FLG promoted a strong genotoxic effect with a LOGEL of 10 µg mL^{-1} while amine-FLG elicited a LOGEL of 50 µg mL^{-1}. 16HBE14o⁻ cells treated with CB particles demonstrated a LOGEL of DNA damage at 20 µg mL^{-1} albeit this genotoxic response produced a higher frequency of micronuclei compared to neutral-FLG. It appears that FLG genotoxicity is reliant upon surface chemistry in conjunction with physical characteristics, such as lateral diameter and thickness. When suspended in 10% supplemented culture media, the agglomerate size for carboxyl-FLG was approximately double those of neutral-FLG, with the former particles bearing only four sheets of graphene as opposed to 50 in neutral-FLG.

Other studies which have compared FLG materials such as Lammel et al. (2013) investigated the cytotoxic effects of graphene oxide and carboxyl graphene nanoplatelets in liver hepatocyte (HepG2) cells. Crucially both materials demonstrated the ability to damage the lipid membrane, invade the cells, and generate ROS in a concentration-dependent manner, initiated as low as 4 µg mL^{-1}. GO at 16 µg mL^{-1} possessed a hydrodynamic diameter of ≈500 nm whereas carboxylated graphene oxide nanoplatelets displayed two separate peak populations at 200 nm and >1 µm.[26] Therefore, when drawing comparisons to the present study, the role of physicochemical features in relation to toxicity becomes apparent. One key aspect of reviewing graphene and FLG genotoxicity is that the particle terminology greatly varies within the literature based upon the authors' interpretation of the physicochemical features. The role of particle uptake and toxicity has been extensively reported in the literature.[26,27] Liao and colleagues showed A549 cells were capable of internalizing rGO into vesicles (shown by TEM) at concentrations up to and including 20 µg mL^{-1}.[28] Uptake in the present study was confirmed by TEM with the 16HBE14o⁻ cells appearing similar to the A549 cells used in the study by Liao and colleagues. The role of surface functionalization did not seem to effect uptake, therefore the importance of surface groups upon the observed genotoxicity in the present study is likely a result of oxidative stress. However, testing the hypothesis of uptake directly effecting toxicity ideally requires evaluation over a long time period, rather than an acute exposure as in the present study whereby no significant cell death was reported after 24 h of exposure.

Several studies have demonstrated the potential of carbonaceous ENMs to promote both clastogenic and aneugenic DNA damage. Muller and colleagues for example demonstrated the potential of multi-walled carbon nanotubes (MWCNTs) to induce both clastogenic and aneugenic events within both an in vivo and in vitro micronucleus assay.[29] The authors targeted type II pneumocytes and also rat lung epithelial cells where it

Table 2. Summary of lowest observed effect levels (LOELs) across biological endpoints, data was considered statistically significant (*) when $p < 0.05$ and $N = 3$.

ENM	Cytotoxicity	Genotoxicity [µg mL^{-1}]	IL-8 Elevation [µg mL^{-1}]	GSH depletion [µg mL^{-1}]	ATP production [µg mL^{-1}]
Neutral-FLG	–	*10	*100	*50	*8
Amine-FLG	–	*50	*100	*50	*4
Carboxyl-FLG	–	–	*50	*50	*2
CB	–	*20	*50	*50	*8

was noted that at 50 μg mL^{-1} a twofold increase in micronuclei was observed and was the result of both clastogenic and aneugenic mechanisms. In the present study, similar findings were noted, where clastogenicity proved to be the prevailing genotoxic mechanism with amine-FLG promoting a significant threefold increase over control levels. Patlolla and colleagues focused on the genotoxic effects of carbonaceous ENMs in an in vivo bone marrow micronucleus assay in Swiss–Webster mice, comparing functionalized (COOH groups) versus non-functionalized MWCNTs with CB as a positive control.[30] The authors reported that functionalized MWCNTs were significantly clastogenic, more so than non-functionalized MWCNTs. These results conflict with the genotoxicity observed in the present study where carboxylated-FLG did not induce genotoxicity. Crucially, in the present study, non-fibrous ENMs were utilized in an in vitro exposure whereby chronic effects or secondary mechanisms could have been undetected. However, to test this hypothesis, the same cells and exposure conditions could be applied to a co-culture of 16HBE14o$^-$ cells, as done by Evans and colleagues.[31]

The potential of graphene ENMs to promote oxidative stress has been highlighted in the literature; this process arises through antioxidant depletion, increases in ROS generation, lipid peroxidation, or mitochondrial stress. The noticeable effect of each ENM upon mitochondrial function relied upon (i) gaining access to the cell cytosol and (ii) interference with the mitochondrial membrane potential, with this effect becoming greater the more oxidized the ENM (evident with carboxyl-FLG and CB particles specifically). The mechanisms of graphene toxicity within mammalian cells have been suggested to be driven by an overproduction of ROS linked to mitochondrial depolarization, which is exacerbated with pristine isotypes of graphene ENMs as opposed to functionalized variants.[14] Theoretical calculations on graphene sheet diameters by Zhou and colleagues demonstrated that a diameter greater than 6.7 nm of graphene would conduct electrons better than electron acceptor sites within the mitochondria, 4Fe4S iron–sulfur clusters.[32] The reduction of which may be impaired by graphene electron conduction, explaining the impairment of ATP production in the present study specifically for carboxyl-FLG. The underlying mechanisms contributing to ATP impairment and mitochondrial membrane potential decreases has been explored, where it has been hypothesized that graphene ENMs can act as electron donors, ramping up electron supply through complexes I and II of the electron transport chain (ETC); thus accelerating the supply of ROS to the cell.[33] This does not appear to be the case in the present study where ENM treatment of 16HBE14o$^-$ cells depleted oxygen consumption suggesting alternative mechanisms of oxidative stress. Furthermore, Zhang and colleagues utilized the nematode as a model to test the hypothesis that GO with low oxidation states proved more damaging via oxidative stress than highly oxidized graphene.[34] The functionalized COOH groups demonstrated a critical effect on the decomposition of H_2O_2 into hydroxyl radicals contributing largely to indirect oxidative stress on the cell, this finding was supported with electron spin resonance spectrometry. This finding correlates with the oxidizing potential of the ENMs in this investigation, (amine-FLG > carboxyl-FLG > CB > neutral-FLG), suggesting neutral-FLG as the most reduced of the ENMs. The identification of the specific functionalities of each FLG material in the present study represents an ideal opportunity for future work. This is particularly relevant to amine-FLG which possesses a higher (negative) zeta potential than neutral-FLG and carboxyl-FLG. In the study by Stueckle and colleagues, MWCNTs obtained from the same supplier, Perpetuus Carbon Technologies (PCT) and also functionalized with amine groups similarly displayed net negative zeta potentials in water. Here however the authors identified additional functional groups such as N—H, O=C, and C=N.[35] Such groupings present on the amine-FLG used in the present study could be responsible for the same net negative response.

The lung employs crucial antioxidant mechanisms for neutralizing ROS, both enzymatic and non-enzymatic.[36] Graphene ENMs have been implicated in the depletion of intracellular glutathione that correlates with a significant increase in intracellular ROS and mitochondrial membrane destabilization.[37] This effect was however stronger in alveolar A549 cells as opposed to BEAS-2B cells indicating either (i) the levels of intracellular GSH differs between lung cell types or (ii) alveolar cells are more readily affected by the oxidative capabilities of graphene ENMs. Further work would be required however to elucidate the link between oxidative stress and the subsequent release of (pro)-inflammatory mediators. The 16HBE14o$^-$ cell exposures could be repeated with an addition of glutathione. Potentially this could identify if additional glutathione can pre-emptively downregulate the (pro)-inflammatory response and lower the oxidative stress and genotoxic response in 16HBE14o$^-$ cells, a hypothesis discussed by Schinwald and colleagues.[38] This concept has been explored by Qian and colleagues whereby the additional supplementation of glutathione decreased the serum levels of TNF-α, IL-6, IL-8, and TGF-β in patients with chronic hepatitis B after 1200 mg of glutathione had been intravenously administered.[39] This indicated a favorable effect of increased serum levels of glutathione. The present study has demonstrated the importance of utilizing a human bronchial lung monoculture to assess the genotoxicity of industrially relevant FLG and CB particles. The data has highlighted that these carbonaceous ENMs can promote DNA damage via primary-indirect mechanisms evident in the depletion of intracellular GSH, decrease in oxygen consumption and ATP production. This resulted in oxidative stress contributing to both clastogenic and aneugenic chromosomal damage with neutral-FLG and amine-FLG. The importance of surface chemistry has been observed in the present study with carboxyl groups appearing to be favorable in mitigating a genotoxic response at high concentrations up to and including 100 μg mL^{-1}. However, 16HBE14o$^-$ exposures to carboxyl-FLG did warrant a (pro)-inflammatory response with IL-8 at high concentrations and produced the strongest effect upon the mitochondria suggesting oxidative stress could be one of numerous mechanisms influencing FLG toxicity in human bronchial epithelial cells.

4. Conclusion

This work has demonstrated the significance of FLG surface chemistry and morphology with regard to carbon ENMs in governing genotoxicity in 16HBE14o$^-$ cells. Neutral-FLG promoted the greatest genotoxic response in 16HBE14o$^-$ cells. Carboxyl groups decreased the thickness (theoretical layer number) and produced the smallest hydrodynamic diameter in both

water and 10% supplemented culture media. These physicochemical features of carboxyl-FLG appear to be decisive in dictating the genotoxicity of the FLG. However, all tested ENMs were able to promote a significant IL-8 response, deplete GSH levels, and demonstrate a potent ability to interfere with mitochondrial function. Carboxyl-FLG, while able to deplete mitochondrial function, induced no significant DNA damage. In the 16HBE14o$^-$ monoculture system, primary indirect genotoxicity was promoted by CB > neutral-FLG > amine-FLG. Carboxyl-FLG therefore appears the optimal functionalization of the ENMs tested where occupational nano-safety is concerned. How this in vitro response correlates to complex in vitro models, in vivo models, and organ systems is uncertain, however. Thus, advising on the nano-safety of these ENMs will require substantial follow-up experimentation; however, the results observed in the present study could provide a strong foundation to be further investigated.

5. Experimental Section

Preparation of ENMs: Neutral-, amine-, and carboxyl-FLG were manufactured via dielectric barrier discharge of mined graphite by Perpetuus Carbon Technologies (PCT, UK). CB particles were sourced from (FLAMMRUSS 101, Lamp Black #8235102) Evonik Degussa Inorganic Materials, Frankfurt. All ENMs were supplied as powder and were suspended at a stock concentration of 10 mg mL^{-1} in double distilled water. Prior to exposures or physicochemical characterization where applicable, ENMs were sonicated in a 90 W ultrasonic bath (Fisher Scientific #FB15046) for 20 min at 37 °C to encourage destabilization of agglomerate material. ENM interference was considered for each endpoint, with careful measures taken to select the appropriate assays thus providing a comprehensive biological interpretation.

Agglomerate Analysis by Plunge-Freeze Scanning Electron Microscopy (SEM): ENMs were prepared at 100 µg mL^{-1} in supplemented (10% fetal bovine serum (FBS)) culture media following a 20-min sonication (90 W ultrasonic bath for 20 min at 37 °C (Fisher Scientific #FB15046)) of stock ENMs. Plunge-freezing of samples followed by vacuum sublimation to capture the agglomerates from solution (as traditional drop cast preparation induced artefacts) was performed as previously detailed by Evans et al.[31] Agglomerates were considered so if the corners or edges of aggregate particles were in physical contact with one another. Samples were imaged by SEM using a Hitachi SU8230 cold field emission gun SEM operating at 15 kV.

Dry Powder SEM and Energy Dispersive X-Ray (EDX) Elemental Composition Analysis: The dry powder ENMs were loaded onto a disposable adhesive pad before being mounted onto an aluminum stub (SEM Clip; 32 mm × 10 mm × M4 (3 clips)) (Agar Scientific). The sample was inserted into the SEM vacuum chamber, then positioned in the electron beam path. Analysis was performed at a tilt angle of 20° using the Hitachi Ultra High-Resolution field emission (FE)-SEM model number: S-4800, $N = 1$.

Atomic Force Microscopy (AFM): To produce topographical images of the FLG and investigate the thickness of agglomerates, water-suspended stock ENM was diluted with ultrapure H_2O to 100 µg mL^{-1}, deposited onto an air-brushed mica slide and analyzed using a Bruker Dimension Icon AFM. A diamond tapping tip (Bruker tip MPP21000 RSFP 3 N m^{-1}) and the SCANASYST-AIR image-optimization scanning (tapping) mode were used to image the samples. Parameters for all measurements were: thickness (T): 650 nm, length (L): 115 µm, width (W): 25 µm, resonance frequency (f_0): 70 kHz, spring constant (k): 0.4 N m^{-1}. Topographical images were analyzed for differences between materials and quantifying layer number with the Bruker Nanoscope Analysis Package version 1.4.

Determination of Purity and Layer Number by Raman Spectroscopy: ENMs were investigated for their layer number, surface impurities, and structural integrity via Raman spectroscopy (Renishaw inVia Reflex Spectrometer System for Raman spectral/imaging analysis) at 533 nm. Each ENM at 100 µg mL^{-1} was dried onto silicon chips. Representative spectra of each FLG material were then generated using the coding package Wolfram Mathematica.

Hydrodynamic Diameter and Surface Charge of Agglomerates: The polydispersity index (PDI), hydrodynamic diameter, and zeta potential were determined using a Malvern Zetasizer Nano ZS (Malvern Instruments, UK) at a wavelength setting of 250 nm following the set parameters outlined by Evans et al.[31] The data was analyzed with the Malvern Zetasizer software version 7.02.

Acellular Production of Superoxide (O_2^-) Radicals: To provide an accurate measure of the FLG ENMs reactivity, electron paramagnetic resonance (EPR) was used to establish oxygen-centered free radical generation by the method previously reported by Miller et al.[40] Stock FLG samples for EPR were suspended in 500 µL of physiological saline solution (Krebs buffer: 118.4 × 10^{-3} M NaCl, 25 × 10^{-3} M $NaHCO_3$, 11 × 10^{-3} M glucose, 4.7 × 10^{-3} M KCl, 1.2 × 10^{-3} M $MgSO_4$, 1.2 × 10^{-3} M KH_2PO_4, 2.5 × 10^{-3} M $CaCl_2$) at concentrations of 3.2–180 µg mL^{-1}. The FLG samples were then incubated with a spin-trap, Tempone-H (1 × 10^{-3} M; Enzo Life Sciences, Exeter, UK), immediately before the initial measurement. Tempone-H is a highly sensitive spin-trap that shows selectivity for superoxide, forming a stable product that can be measured by EPR.[41] Pyrogallol (32 × 10^{-6} M) was used as a positive control to spontaneously generate superoxide radicals in Krebs buffer.[42]

Cell Culture: The bronchial cell-line 16HBE14o$^-$ was kindly donated by Professor D. C. Gruenert, University of California, San Francisco, USA. The cells were cultured (doubling time of 22 h) in MEM containing 10% L-glutamine and supplemented with 10% FBS and 1% streptomycin/penicillin. Culture flasks were pre-coated with fibronectin solution before cell seeding; 88% LHC basal medium, 10% 1 mg mL^{-1} BSA, 1% 3 mg mL^{-1} bovine collagen, and 1% 1 mg mL^{-1} human fibronectin.

Confirmation of Cellular Interaction/Entry Using Transmission Electron Microscopy (TEM): ENM cellular uptake was confirmed by TEM imaging. 16HBE14o$^-$ cells exposed to ENM were fixed, embedded, sectioned, and imaged as previously described.[43] The analysis was performed with a FEI Titan^3 Themis G2 operating at 300 kV fitted with 4 EDX silicon drift detectors, and a Gatan One-View CCD. EDX spectroscopy and mapping was undertaken using Bruker Esprit v1.9 software.

Cytotoxicity by Relative Population Doubling (RPD) and Genotoxicity: 16HBE14o$^-$ cells were seeded at 1.0 × 10^5 cells mL^{-1} in T25 (25 cm^2) flasks and allowed to adhere and grow for 24 h after which the cells at 70–80% confluency were then treated with a vehicle control (cell culture media alone) and ENMs for 24 h. Mitomycin-C (MMC) at 0.01 µg mL^{-1} was used as the positive control, the assay was performed as previously detailed by Evans et al.[31] All experiments were performed in triplicate ($n = 3$) and 2000 binucleate (BN) cells per replicate were scored per concentration (6000 BN cells in total). To determine if the DNA damage induced was a consequence of an aneugenic or clastogenic response, following the cytokinesis blocked micronucleus (CBMN) assay treatment, 16HBE14o$^-$ cells were cytocentrifuged (500g for 5 min) onto slides and fixed in 90% methanol at −20 °C. Immunofluorescent staining of kinetochore proteins was performed as described by Singh and colleagues.[44] Kinetochore scoring was carried out on a Zeiss AxioCam HRc (Carl Zeiss Microscopy and Imaging, UK). For each concentration, micronuclei from 105 binucleated cells (35 per replicate) were scored for the presence or absence of kinetochore signals.

(Pro)-Inflammatory Response: Supernatant from the CBMN assay was harvested following 16- and 24-h exposure to ENMs and analyzed using an IL-8 enzyme-linked immunosorbent assay (ELISA) (DuoSet ELISA; R&D Systems Europe). ELISAs were performed in triplicate following the manufactures instructions. The optical density (OD) was recorded at a wavelength set to 450 nm with an Omega Multimode microplate reader (BMG LABTECH Ltd, UK). A total of three biological replicates were conducted ($N = 3$).

Antioxidant Depletion: 16HBE14o$^-$ cells were seeded at 1.0 × 10^5 cells mL^{-1} and allowed to adhere for 24 h, after which the cells were then treated with ENMs for 24 h. Following both 6- and 24-h exposures, 16HBE14o$^-$ cells were washed twice with PBS, harvested and lysed to

extract intracellular glutathione (GSH). Fluorescence spectroscopy of monochlorobimane was performed with set parameters of 390 nm (excitation) and 478 nm (emission). The assay was performed as per the manufacturer's instructions (Sigma-Aldrich, UK) in black-sided 96 well plates, Nunc FuoroNunc. Data was normalized through quantification of cellular protein utilizing the DC assay (Bio-Rad, UK) and a series of bovine serum albumin (BSA) (Bio-Rad, UK) standards prepared using RIPA buffer (Thermo Scientific, UK). The plate was then read on a FLUOstar OMEGA Multimode microplate reader (BMG, LABTECH Ltd, UK). Total cellular protein measurements were used to normalize all data sets ($N = 3$).

Mitochondrial Stress and Bioenergetics: 16HBE14o$^-$ cells were seeded at 120×10^3 cells mL^{-1} (100 µL per well) into XFe24 tissue culture plates (Seahorse Bioscience). The following day, cells were topped up with growth media (150 µL) and exposed to ENMs for 24 h over the full range of 0, 2, 4, 8, 10, 20, 50, and 100 µg mL^{-1}. The assay was performed as detailed by Jones and colleagues.[45] Data was normalized through quantification of cellular protein (DC assay (Bio-Rad, UK)) and a series of BSA (Bio-Rad, UK) standards (2, 1.5, 1, 0.5, and 0 mg mL^{-1}) prepared using RIPA buffer (Thermo Scientific, UK). All experiments were conducted in triplicate.

Statistics: All data is presented as the mean ± the standard deviation (SD). Statistical analysis was performed in SPSS statistics software (v.20 IBM, UK) where all data sets were first analyzed for normality (Shapiro-Wilk test, $p \leq 0.05$) and for equal variance $p \leq 0.05$). A one-way analysis of variance (ANOVA) was performed with post hoc Dunnett's multiple comparisons applied to evaluate pairwise statistical significance between control and concentrations; the alpha value was set to 0.05. If data was not normally distributed the T3 or Dunn's test was applied.

Supporting Information

Supporting Information is available from the Wiley Online Library or from the author.

Acknowledgements

This work was jointly supported by the European Social Fund (ESF) through the Welsh Government; Knowledge Economy Skills Scholarships (KESS2 (Grant #80815)) and Perpetuus Carbon Technologies (PCT). M.M. is funded by the British Heart Foundation (SP/15/8/31575; CH/09/002).

Conflict of Interest

The authors declare no conflict of interest.

Author Contributions

M.J.B., M.J.D.C., and S.H.D. designed the experiments. M.J.B. performed cell culture and all toxicological assays described. M.J.B. and S.J.E. performed DLS and Zeta Potential analysis. N.H. performed plunge-freeze SEM & TEM. M.M. evaluated extracellular production of superoxide radicals using EPR. A.W. analyzed FLG samples via Raman spectroscopy and produced Raman supplementary figure. S.B.L. captured AFM images. A.T. provided FLG samples and contributed to characterization and data interpretation. All authors contributed to data interpretation and preparation of manuscript.

Keywords

genotoxicity, graphene, in vitro, lung, nano

Received: April 22, 2020
Revised: June 5, 2020
Published online: July 30, 2020

[1] S. Arora, J. M. Rajwade, K. M. Paknikar, *Toxicol. Appl. Pharmacol.* **2012**, *258*, 151.
[2] European Commission, *Off. J. Eur. Union.* **2011**, *L275*, 38.
[3] G. Oberdorster, A. Maynard, K. Donaldson, V. Castranova, J. Fitzpatrick, K. Ausman, J. Carter, B. Karn, W. Kreyling, D. Lai, S. Olin, N. Monteiro-Riviere, D. Warheit, H. Yang, ILSI Research Foundation/Risk Science Institute Nanomaterial Toxicity Screening Working Group, *Part. Fibre Toxicol.* **2005**, *2*, 8.
[4] R. Gupta, H. Xie, *J. Environ. Pathol. Toxicol. Oncol.* **2018**, *37*, 209.
[5] V. Stone, M. R. Miller, M. J. D. Clift, A. Elder, N. L. Mills, P. Møller, R. P. F. Schins, U. Vogel, W. G. Kreyling, K. A. Jensen, T. A. J. Kuhlbusch, P. E. Schwarze, P. Hoet, A. Pietroiusti, A. D. Vizcaya-Ruiz, A. Baeza-Squiban, J. P. Teixeira, C. L. Tran, F. R. Cassee, *Environ. Health Perspect.* **2017**, *125*, 106002.
[6] B. Fadeel, C. Bussy, S. Merino, E. Vázquez, E. Flahaut, F. Mouchet, L. Evariste, L. Gauthier, A. J. Koivisto, U. Vogel, C. Martín, L. G. Delogu, T. Buerki-Thurnherr, P. Wick, D. Beloin-Saint-Pierre, R. Hischier, M. Pelin, F. C. Carniel, M. Tretiach, F. Cesca, F. Benfenati, D. Scaini, L. Ballerini, K. Kostarelos, M. Prato, A. Bianco, *ACS Nano* **2018**, *12*, 10582.
[7] E. Bressan, L. Ferroni, C. Gardin, L. Sbricoli, L. Gobbato, F. Ludovihetti, I. T. Tussardi, A.Carraro, A. Piattelli , B. Zavan, *J. Transl. Med.* **2014**, *12*, 296.
[8] Y. Zhang, Y. W. Tan, H. L. Stormer, P. Kim, *Nature* **2005**, *438*, 201.
[9] A. A. Balandin, S. Ghosh, W. Bao, I. Calizo, D. Teweldebrhan, F. Miao, C. N. Lau, *Nano Lett.* **2008**, *8*, 902.
[10] C. Lee, X. Wei, J. W. Kysar, J. Hone, *Science* **2008**, *321*, 385.
[11] C. Mathioudakis, P. C. Kelires, *Nanoscale Res. Lett.* **2016**, *11*, 151.
[12] G. Li, Y. Yang, R. Zhou, F. Meng, X. Li, *Eur. J. Pharm. Sci.* **2018**, *123*, 249.
[13] V. C. Sanchez, A. Jachak, R. H. Hurt, A. B. Kane, *Chem. Res. Toxicol.* **2012**, *25*, 15.
[14] A. Jarosz, M. Skoda, I. Dudek, D. Szukiewicz, *Oxid Med Cell Longevity* **2016**, *2016*, 5851035.
[15] Y. Zhang, S. F. Ali, E. Dervishi, Y. Xu, Z. Li, D. Casciano, A. S. Biris, *ACS Nano* **2010**, *4*, 3181.
[16] Y. Li, Y. Liu, Y. Fu, T. Wei, L. L. Guyader, G. Gao, R.-S. Liu, Y.-Z. Chang, C. Chen, *Biomaterials* **2012**, *33*, 402.
[17] C. Liao, Y. Li, S. C. Tjong, *Int. J. Mol. Sci.* **2018**, *19*, 3564.
[18] X . Hu, H. Lei, X. Zhang, Y. Zhang, *Microsc. Res. Tech.* **2016**, *79*, 721.
[19] C. E. Stewart, E. E. Torr, N. H. Mohd Jamili, C. Bosquillon, I. Sayers, *J. Allergy (Cairo)* **2012**, *2012*, 943982.
[20] S. Bengtson, K. Kling, A. M. Madsen, A. W. Noergaard, N. R. Jacobsen, P. A. Clausen, B. Alonso, A. Pesquera, A. Zurutuza, R. Ramos, H. Okuno, J. Dijon, H. Wallin, U. Vogel, *Environ. Mol. Mutagen.* **2016**, *57*, 469.
[21] S. Dikalov, M. Skatchkov, E. Bassenge, *Biochem. Biophys. Res. Commun.* **1997**, *230*, 54.
[22] A. Don Porto Carero, P. H. Hoet, L. Verschaeve, G. Schoeters, B. Nemery, *Environ. Mol. Mutagen.* **2001**, *37*, 155.
[23] I. L. Hsiao, Y. J. Huang, *J. Nanopart. Res.* **2013**, *15*, 1829.
[24] J. W. Wills, H. D. Summers, N. Hondow, A. Sooresh, K. E. Meissner, P. A. White, P. Rees, A. Brown, S. H. Doak, *ACS Nano* **2017**, *11*, 11986.
[25] N. Singh, G. J. Jenkins, S. M. Griffiths, P. M. Williams, T. G. G. Maffeis, C. J. Wright, S. H. Doak, *Biomaterials* **2009**, *30*, 3891.
[26] T. Lammel, P. Boisseaux, M. L. Fernandez-Cruz, J. M. Navas, *Part. Fibre Toxicol.* **2013**, *10*, 27.
[27] W. Zhang, L. Yan, M. Li, R. Zhao, X. Yang, T. Ji, Z. Gu, J.-J. Yin, X. Gao, G. Nie, *Toxicol. Lett.* **2015**, *237*, 61.
[28] Y. Liao, W. Wang, X. Huang, Y. Sun, S. Tian, P. Cai, *Sci. Rep.* **2018**, *8*, 15188.
[29] J. Muller, I. Decordier, P. H. Hoet, N. Lombaert, L. Thomassen, F. Huaux, D. Lison, M. Kirsch-Volders, *Carcinogenesis* **2008**, *29*, 427.

[30] A. K. Patlolla, S. M. Hussain, J. J. Schlager, S. Patlolla, P. B. Tchounwou, *Environ. Toxicol.* **2010**, *25*, 608.
[31] S. J. Evans, M. J. D. Clift, N. Singh, J. W. Wills, N. Hondow, T. S. Wilkinson, M. J. Burgum, A. P. Brown, G. J. Jenkins, S. H. Doak, *Part. Fibre Toxicol.* **2019**, *16*, 8.
[32] H. Zhou, B. Zhang, J. Zheng, M. Yu, T. Zhou, K. Zhao, Y. Jia, X. Gao, C. Chen, T. Wei, *Biomaterials* **2014**, *35*, 1597.
[33] B. Zhang, P. Wei, Z. Zhou, T. Wei, *Adv. Drug Delivery Rev.* **2016**, *105*, 145.
[34] W. Zhang, C. Wang, Z. Li, Z. Lu, Y. Li, J.-J. Yin, Y.-T. Zhou, X. Gao, Y. Fang, G. Nie, Y. Zhao, *Adv. Mater.* **2012**, *24*, 5391.
[35] T. A. Stueckle, D. C. Davidson, R. Derk, P. Wang, S. Friend, D. Schwegler-Berry, P. Zheng, N. Wu, V. Castranova, Y. Rojanasakul, L. Wang, *Nanotoxicology* **2017**, *11*, 613.
[36] A. J. Thorley, T. D. Tetley, *Int. J. Chronic Obstruct. Pulmon. Dis.* **2007**, *2*, 409.
[37] A. Schinwald, F. A. Murphy, A. Jones, W. MacNee, K. Donaldson, *ACS Nano* **2012**, *6*, 736.
[38] L. Qian, W. Wang, Y. Zhou, J. Ma, *Cent. Eur. J. Immunol.* **2017**, *42*, 97.
[39] E. L. Taylor, A. G. Rossi, C. A. Shaw, F. P. Dal Rio, C. Haslett, I. L. Megson, *Br. J. Pharmacol.* **2004**, *143*, 179.
[40] M. R. Miller, S. J. Borthwick, C. A. Shaw, S. G. McLean, D. McClure, N. L. Mills, R. Duffin, K. Donaldson, I. L. Megson, P. W. F. Hadokel, D. E. Newby, *Environ. Health Perspect.* **2009**, *117*, 611.
[41] J. W. Wills, N. Hondow, A. D. Thomas, K. E. Chapman, D. Fish, T. G. Maffeis, M. W. Penny, R. A. Brown, G. J. S. Jenkins, A. P. Brown, P. A. White, S. H. Doak, *Part. Fibre Toxicol.* **2016**, *13*, 50.
[42] N. Singh, G. J. Jenkins, B. C. Nelson, B. J. Marquis, T. G. G. Maffeis, A. P. Brown, P. M. Williams, C. J. Wright, S. H. Doak, *Biomaterials 33*, **2012**, 163.
[43] N. Jones, J. Piasecka, A. H. Bryant, R. H. Jones, D. O. F. Skibinski, N. J. Francis, C. A. Thornton, *Clin. Exp. Immunol.* **2015**, *182*, 69.
[44] Y. Chang, S. T. Yang, J. H. Liu, E. Dong, Y. Wang, A. Cao, Y. Liu, H. Wang, *Toxicol. Lett.* **2011**, *200*, 201.
[45] S. Mittal, V. Kumar, N. Dhiman, L. K. Chauhan, R. Pasricha, A. K. Pandey, *Sci. Rep.* **2016**, *6*, 39548.